Shock-Capturing Technique for Hypersonic, Chemically Relaxing Flows

Scott Eberhardt*
University of Washington, Seattle, Washington
and
Kevin Brown†
NASA Ames Research Center, Moffett Field, California

A fully coupled, shock-capturing technique is presented for chemically reacting flows at high Mach numbers. The technique makes use of a total variation diminishing (TVD) dissipation operator that results in sharp, crisp shocks. The eigenvalues and eigenvectors of the fully coupled system, which includes species conservation equations in addition to the gasdynamics equations, are analytically derived for a general reacting gas. Species production terms for a model dissociating gas are introduced and are included in the algorithm. The convective terms are also solved using a first-order TVD scheme, while the source terms are solved using a fourth-order Runge-Kutta scheme to enhance stability. Results from one-dimensional numerical experiments are shown for both a two- and a three-species gas.

Nomenclature

a = speed of sound
A = flux Jacobian matrix, $= \partial F/\partial q$
c_i = species mass fraction of ith species
c_v = specific heat at constant volume
c_{v_i} = specific heat for ith species
C_f = reaction rate coefficient, forward reaction
C_b = reaction rate coefficient, reverse reaction
e = internal energy
E = total energy per unit volume, $= \rho e + \frac{1}{2}\rho u^2$
F = convective flux vector
F_j = flux vector at discrete point j
$\tilde{F}_j$ = TVD flux at j
h_i^0 = heat of formation for ith species
H = total enthalpy per unit mass, $= E + p/\rho$
k_f = forward reaction rate
k_b = reverse reaction rate
m = x momentum
M_i = molecular mass of ith species
p = pressure
q = conservation variables
R = universal gas constant
t = time
T = temperature
TVD = total variation diminishing
u = velocity
W = source term for species production
x = x coordinate
X = eigenvectors of A
X^{-1} = inverse of X
α = characteristic variables
n_f = exponent for forward reaction
n_b = exponent for reverse reaction
Θ_d = heat of reaction
λ^l = lth eigenvalue
Λ = matrix of eigenvalues
ρ = density
ϕ^l = elements of Φ
Φ = TVD dissipation operator
ψ = numerical viscosity term

Subscripts

A = species A
A_2 = molecule A_2
B = species B
b = backward (reverse) reaction
f = forward reaction
i = species index
j = grid index
ns = number of species

Presented as Paper 86-0231 at the AIAA 24th Aerospace Sciences Meeting, Reno, NV, Jan. 6–9, 1986; received Jan. 27, 1986; revision received Oct. 22, 1986.

*Assistant Professor, Department of Aeronautics and Astronautics. Member AIAA.
†Captain, U.S. Air Force. Member AIAA.

Introduction

THE development of a class of advanced space transportation systems over the next few decades will require new numerical techniques to aid to their design The most publicized of these systems is the aeroassisted orbital transfer vehicles (AOTV). These vehicles are proposed by NASA to carry payloads from one orbit to another using aerodynamic forces in the upper atmosphere to accomplish orbital altitude or inclination changes. A detailed mission analysis of AOTV can be found in Ref. 1.

The design of AOTV's will require detailed knowledge of the low-density, hypervelocity flowfield where the vehicle is expected to maneuver. There are strong indications that the flow will be in chemical nonequilibrium, which can greatly influence heating rates to the vehicle. Howe[2] gives an introduction to aerothermodynamic problems related to AOTV concepts.

The design of the AOTV cannot be accomplished with accuracy without the development of some new computational tools. The new capabilities that will be required include the ability to capture strong shocks (over Mach 20), the ability to resolve regions of strong expansion, and the ability to handle real-gas effects, such as chemical nonequilibrium. Figure 1 illustrates these flow features on a generic AOTV. The strong

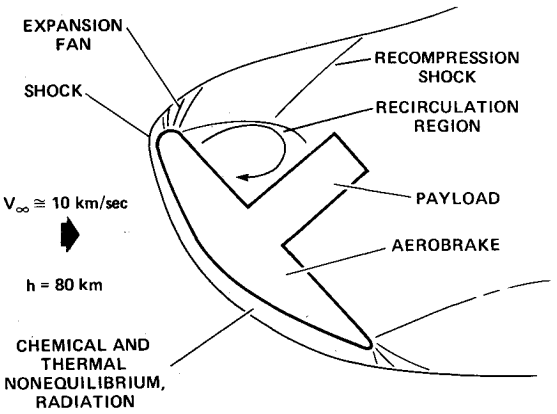

Fig. 1 AOTV flowfield.

bow shock may be fitted by shock fitting techniques, but the resolution of internal recompression shocks will require shock-capturing capabilities. The flow behind the shock wave will be in chemical and thermal nonequilibrium, which has the effect of reducing the shock stand-off distance found in the nonreacting-gas case. In addition, the nonequilibrium effects will affect the solution during the expansion to the base flow region. Resolving these complex physical phenomenon will be a great challenge for computational aerothermodynamics.

The goal of this paper is to develop an algorithm that can capture discontinuities and allow for finite-rate chemistry so that it can eventually be applied to the AOTV. This study extends a current shock-capturing, ideal-gas algorithm[3,4] to include chemical nonequilibrium effects and applies it to a one-dimensional shock wave. The one-dimensional problem serves as a vehicle to study the addition of the finite-rate chemistry to the Euler equations of gasdynamics. Clearly, the complete AOTV problem requires a multidimensional code with diffusion terms included; however, model problems must be tested first to achieve an appropriate level of confidence.

A total variation diminishing (TVD) numerical dissipation operator is used to produce sharp and crisp shocks. The scheme fully couples the gasdynamic equations with species conservation equations. As used here, fully coupled implies that the species conservation equations are solved using the same integration procedure as the gasdynamics equations. In particular, this means using the eigensystem for the complete set of equations, rather than for the gasdynamics alone, when determining propagation speeds for the TVD operator. The species conservation equations, which must be added to account for the finite-rate chemistry, have convective flux terms that modify the characteristic nature of the system and the equations contain source terms to account for species production. Note that the species conservation equations account for species consumed or produced in finite-rate reactions and implies that all of a species in a cell volume is either convected across cell walls or is involved in a mass conservative reaction. This differs from the strong conservation law form, which would include no source terms and, therefore, no reactions. In this work, a model real gas is used where each species exhibits individual properties (i.e., molecular mass and specific heats).

Other studies that compute chemical nonequilibrium flows generally uncouple the species equations from the gasdynamics equations. However, a few researchers have solved the equations completely coupled. Park[5] solved an 11 species shock-tube problem using a shock-fitting, central-differenced, implicit scheme. His coupled scheme was computationally costly and was inadequate for stable, robust solutions, particularly in the regions where the chemical reaction times were fast and the gradients high. In two other studies, Carofano[6] and Bussing and Murman[7] have also coupled species equations with gasdynamics equations, but have applied their solutions to combustion problems at lower Mach numbers. This study introduces a model real gas with up to three species and investigates the coupling species equations to gasdynamics equations. In addition to solving the completely coupled set of equations, an alternate form of the scheme is introduced that uses this coupling information to reduce the computation time.

Equations

The equations for the one-dimensional, inviscid, reacting-gas model are solved in conservation law form. The equations represent conservation of species, mixture momentum, and total mixture energy, all per unit volume. The equations are usually written

$$\frac{\partial q}{\partial t} + \frac{\partial F}{\partial x} = W \tag{1}$$

The vectors q, F, and W are defined by

$$q = \begin{bmatrix} \rho_1 \\ \rho_1 \\ \vdots \\ \rho_{ns} \\ m \\ E \end{bmatrix}, \quad F = \begin{bmatrix} c_1 m \\ c_2 m \\ \vdots \\ c_{ns} m \\ \dfrac{m^2}{\rho} + p \\ \dfrac{m}{\rho}(E+p) \end{bmatrix}, \quad W = \begin{bmatrix} w_1 \\ w_2 \\ \vdots \\ w_{ns} \\ 0 \\ 0 \end{bmatrix} \tag{2}$$

The viscous, or diffusion, terms are not included in this study. The pressure p comes from the state equation for each of the species $[p_i = p_i(\rho_i, T)]$ and Dalton's law $[p = p(p_i) = p(\rho_i, T)]$ and is written as

$$p = \sum_{i=1}^{ns} \frac{\rho_i}{M_i} RT \tag{3}$$

The temperature T is determined from the definition of the total energy,

$$c_v T = \frac{E}{\rho} - \frac{u^2}{2} - \sum_{i=1}^{ns} c_i h_i^0 \tag{4}$$

It is assumed that the gas is in thermal equilibrium; thus, the vibrational temperature and translational temperature are equal. Note that the left-hand side of Eq. (4) should read $\int_0^T c_v(T)\,\mathrm{d}T$, but it has been assumed that the integral can be evaluated to read $c_v T$ for this study.

The terms w_i in Eq. (2) represent the production of species from chemical reactions and will be described later. It should be noted that the sum of the species equations yields mixture mass conservation; therefore, the mixture mass conservation equation is redundant and not solved. If the equations are solved uncoupled, then summing the species finite-difference equations does not guarantee conservation of mass, but may result in a nonconservative form of the mixture mass finite-difference equation. It is speculated that this is a cause of the inconsistencies that arise in uncoupled methods, particularly in high-gradient regions. These inconsistencies can result in wrong answers, so they must be absorbed by a correction procedure. The conservative mixture-mass equation can be solved instead of one of the species equations, but this approach is not taken because of added complexity to the flux Jacobian matrix and its eigenvectors.

The governing partial differential equations are hyperbolic in nature. A significant amount of research has been done to study the properties of hyperbolic systems similar to Eq. (1) based on an ideal gas. This vast knowledge base can provide useful information in solving chemically reacting flows.

Algorithm

An explicit method was chosen to develop a simple understanding of the important terms present in the equations without introducing the complications with an implicit method.

Implicit schemes generally have greater stability characteristics and are usually favored for stiff equations such as those used here. However, implicit schemes generally require block matrix inversions, which are computationally expensive. A three-dimensional, ideal-gas equation set will generally have 5×5 blocks, which can be handled on today's computers. An 11 species gas in three dimensions will have 15×15 blocks, which is currently beyond the capabilities of today's computers for realistic problems. Methods to reduce the block size may be possible and represent an area of future research.

The difference of the convective flux terms and the source terms are handled differently. The flux terms use an explicit differencing with a TVD dissipation model for numerical damping. The source terms are evaluated using a fourth-order, Runge-Kutta differencing in time to enhance stability. The complete algorithm is written

$$q_j^{n+1} = q_j^n - \frac{\Delta t}{\Delta x}\left(\tilde{F}^n_{j+\frac{1}{2}} - \tilde{F}^n_{j-\frac{1}{2}}\right) + \frac{\Delta t}{6}\left(W_j^n + 2\tilde{W}_j + 2\tilde{\tilde{W}}_j + \tilde{\tilde{\tilde{W}}}_j\right) \tag{5}$$

where $\tilde{F}_{j+\frac{1}{2}}$ will be discussed in the following section and

$$\begin{aligned} \bar{q}_j &= q_j^n + \tfrac{1}{2}\Delta t W_j^n, & \tilde{W} &= \tilde{W}(\bar{q}) \\ \tilde{\bar{q}}_j &= q_j^n + \tfrac{1}{2}\Delta t \tilde{W}_j, & \tilde{\tilde{W}} &= \tilde{\tilde{W}}(\tilde{\bar{q}}) \\ \tilde{\tilde{\bar{q}}}_j &= q_j^n + \Delta t \tilde{\tilde{W}}_j, & \tilde{\tilde{\tilde{W}}} &= \tilde{\tilde{\tilde{W}}}(\tilde{\tilde{\bar{q}}}) \end{aligned} \tag{6}$$

Convection Terms

Current shock-capturing algorithms contain sophisticated dissipation models to enhance the stability of the solution and are designed to eliminate classical pre- and postshock oscillations. The oscillations that occur with improper dissipation generally become unstable with stronger shocks; therefore, shocks must be captured oscillation free. The dissipation model used in this study has been applied by Yee et al.[8] to a problem with a Mach 10 shock with success. The details of this model, applied to ideal gases, can be found in Refs. 3 and 4.

The governing equations can be reformulated in a more convenient manner for analysis by introducing the flux Jacobian matrix A, where $A = \partial F/\partial q$. The governing equations then become

$$\frac{\partial q}{\partial t} + A\frac{\partial q}{\partial x} = W \tag{7}$$

In this form the methods for solving systems of hyperbolic conservation laws can be studied.

Dissipation models for hyperbolic finite-difference procedures that are successful in capturing strong shocks all make use of the wave properties of the Euler equations. The wave propagation properties are defined by the eigenvalues and eigenvectors of the flux Jacobian matrix, A and are obtained by diagonalizing A, such as

$$A = X\Lambda X^{-1} \tag{8}$$

Because the eigenvalues of A are real, the equations are hyperbolic. Note that it is in the evaluation of A, X, X^{-1}, and Λ where the coupling of the gasdynamic equations with the species conservation equations occur.

A and Λ, for a three-species gas, are

$$A = \begin{bmatrix} u(1-c_1) & -uc_1 & -uc_1 & c_1 & 0 \\ -uc_2 & u(1-c_2) & -uc_2 & c_2 & 0 \\ -uc_3 & -uc_3 & u(1-c_3) & c_3 & 0 \\ P_{\rho 2} - u^2 & P_{\rho 2} - u^2 & P_{\rho 3} - u^2 & 2u + P_m & P_E \\ u(P_{\rho 1} - H) & u(P_{\rho 2} - H) & u(P_{\rho 3} - H) & H + uP_m & u(1 + P_E) \end{bmatrix} \tag{9}$$

and

$$\Lambda = \mathrm{Diag}\left[u, u, u, u + \sqrt{P_\rho + P_E(H - u^2)}, u - \sqrt{P_\rho + P_E(H - u^2)}\right] \tag{10}$$

with

$$\begin{aligned} P_{\rho 1} &= \left(\frac{\partial \rho}{\partial \rho_1}\right)_{\rho 2, \rho 3, m, E}, & P_{\rho 2} &= \left(\frac{\partial p}{\partial \rho_2}\right)_{\rho 1, \rho 3, m, E}, \\ P_{\rho 3} &= \left(\frac{\partial p}{\partial \rho_3}\right)_{\rho 1, \rho 2, m, E}, & P_m &= \left(\frac{\partial p}{\partial m}\right)_{\rho 1, E}, \\ P_E &= \left(\frac{\partial p}{\partial E}\right)_{\rho 1, m}, & P_\rho &= \left(\frac{\partial p}{\partial \rho}\right)_{m, E} \end{aligned} \tag{11}$$

The total enthalpy per unit mass $H = (E + p)/\rho$ is introduced for convenience. The derivatives, which may not be familiar from thermodynamics, are simply derivatives of pressure with respect to the conservative variables of Eq. (2). The set of eigenvalues are generalized from the set for ideal gases, which has introduced a generalized "speed of sound" defined by

$$a^2 = \left(\frac{\partial p}{\partial \rho}\right)_{m, E} + (H - u^2)\left(\frac{\partial p}{\partial E}\right)_{\rho, m}. \tag{12}$$

For analysis, the following relation is derived from the equation of state

$$P_m = -uP_E \tag{13}$$

A relationship has been introduced to determine the eigenvalues based on Dalton's law for partial pressures. The relationship is

$$\left(\frac{\partial p}{\partial \rho}\right)_{m, E} = \sum_{i=1}^{ns} c_i \left(\frac{\partial p}{\partial \rho_i}\right)_{\rho_j, m, E} \tag{14}$$

The expressions for $(\partial p/\partial \rho_i)_{\rho_r, m, E}$ and $(\partial p/\partial E)_{\rho, m}$ are evaluated as

$$\left(\frac{\partial p}{\partial E}\right)_{\rho, m} = \sum_{i=1}^{ns} \frac{\rho_i}{M_i} R c_v$$

$$\left(\frac{\partial p}{\partial \rho_i}\right)_{\rho j, m} = \frac{R}{M_i} T - \frac{p}{\rho}\frac{c_{v_i}}{c_v} + \frac{\Sigma \frac{c_i}{M_i} R}{c_v}\left[\frac{m^2}{2\rho^2} - h_i^0\right] \tag{15}$$

The set of eigenvectors X and its inverse X^{-1} are

$$X = \begin{bmatrix} 1 & 0 & 0 & c_1 & c_1 \\ 0 & 1 & 0 & c_2 & c_2 \\ 0 & 0 & 1 & c_3 & c_3 \\ u & u & u & u + a & u - a \\ u^2 - \frac{P_{\rho 2}}{P_e} & u^2 - \frac{P_{\rho 2}}{P_e} & u^2 - \frac{P_{\rho 3}}{P_e} & H + ua & H - ua \end{bmatrix} \tag{16}$$

$$X^{-1}=\begin{bmatrix} 1-\frac{c_1}{a^2}P_{\rho_1} & -\frac{c_1}{a^2}P_{\rho_2} & -\frac{c_1}{a^2}P_{\rho_3} & u\frac{c_1}{a^2}P_E & -\frac{c_1}{a^2}P_E \\ -\frac{c_2}{a^2}P_{\rho_1} & 1-\frac{c_2}{a^2}P_{\rho_2} & -\frac{c_2}{a^2}P_{\rho_3} & u\frac{c_2}{a^2}P_E & -\frac{c_2}{a^2}P_E \\ -\frac{c_3}{a^2}P_{\rho_1} & -\frac{c_3}{a^2}P_{\rho_2} & 1-\frac{c_3}{a^2}P_{\rho_3} & u\frac{c^3}{a^2}P_E & -\frac{c_3}{a^2}P_E \\ \frac{1}{2a^2}(P_{\rho_1}-ua) & \frac{1}{2a^2}(P_{\rho_2}-ua) & \frac{1}{2a^2}(P_{\rho_3}-ua) & \frac{1}{2a^2}(a-uP_E) & \frac{1}{2a^2}P_E \\ \frac{1}{2a^2}(P_{\rho_1}+ua) & \frac{1}{2a^2}(P_{\rho_2}+ua) & \frac{1}{2a^2}(P_{\rho_3}+ua) & -\frac{1}{2a^2}(a+uP_E) & \frac{1}{2a^2}P_E \end{bmatrix} \tag{17}$$

Extensions of this analysis to N species is clear and involves adding a new eigenvalue u and an eigenvector for each additional equation.

The algorithm and dissipation model for the convective terms used in this study will now be discussed. Yee's algorithm is described, for first-order accuracy, with the source term set to zero, by

$$q^{n+1}=q^n-\frac{\Delta t}{\Delta x}\left(\hat{F}^n_{j+\frac{1}{2}}-\hat{F}^n_{j-\frac{1}{2}}\right) \tag{18}$$

where $x=j\Delta x$ and the numerical flux $\hat{F}^n_{j+\frac{1}{2}}$ is defined as

$$\hat{F}_{j+\frac{1}{2}}=\tfrac{1}{2}\left[F_j+F_{j+1}+X_{j+\frac{1}{2}}\Phi_{j+\frac{1}{2}}\right] \tag{19}$$

The vector F_j is the flux vector of Eq. (2) and the matrix $X_{j+\frac{1}{2}}$ is the set of eigenvectors from Eq. (16) and is evaluated at the midpoint of j and $j+1$. The vector $\Phi_{j+\frac{1}{2}}$ is obtained in the following way. First, define

$$\alpha_{j+\frac{1}{2}}=X^{-1}_{j+\frac{1}{2}}(q_{j+1}-q_j) \tag{20}$$

Also let

$$\psi\left(\lambda^l_{j+\frac{1}{2}}\right)=|\lambda^l_{j+\frac{1}{2}}|, \qquad \lambda^l_{j+\frac{1}{2}}>\epsilon \tag{21}$$

$$=\frac{1}{2\epsilon}\left(\lambda^{l}_{j+\frac{1}{2}2}+\epsilon 2\right), \qquad \lambda^l_{j+\frac{1}{2}}\le\epsilon \tag{22}$$

where $\lambda^l_{j+\frac{1}{2}}$ are the eigenvalues of A evaluated at $j+\frac{1}{2}$. Now, the elements of $\Phi_{j+\frac{1}{2}}$ can be determined by

$$\phi^l_{j+\frac{1}{2}}=-\psi\left(\lambda^l_{j+\frac{1}{2}}\right)\alpha^l_{j+\frac{1}{2}} \tag{23}$$

The dissipation model has the effect of creating an upwind differencing to the central differenced scheme. The dissipation operator, formulated for first-order accuracy, as it is in this study, is approximately defined by

$$X_{j+\frac{1}{2}}\Phi_{j+\frac{1}{2}}\approx-|A|(q_{j+1}-q_j) \tag{24}$$

where $|A|$ is defined as $X|\Lambda|X^{-1}$ and $|\Lambda|$ is the matrix of absolute values of the eigenvalues. This is standard CFD terminology to define a flux splitting scheme. If no dissipation model were added to $\hat{F}_{j+\frac{1}{2}}$, then the algorithm is simply central differencing in space. Adding $X_{j+\frac{1}{2}}\Phi_{j+\frac{1}{2}}$ to $F_{j+\frac{1}{2}}$ makes the algorithm effectively upwind, such as

$$\lambda_l>0, \text{ then } \tilde{F}_{j+\frac{1}{2}}-\tilde{F}_{j-\frac{1}{2}}\approx F_j-F_{j-1}$$

$$\lambda_l<0, \text{ then } \tilde{F}_{j+\frac{1}{2}}-\tilde{F}_{j-\frac{1}{2}}\approx F_{j+1}-F_j \tag{25}$$

The dissipation model can easily be extended to second-order-accurate differencing of the flux terms for ideal gases, but so far there has been no success for the real reacting gas studied here.

This method for computing the convective terms results in a fully coupled, conservation formulation for solving reacting-gas problems. The algorithm does decouple convective waves to determine fluxes; however, these waves are determined from the completely coupled system. In contrast, if the two equation sets are solved decoupled (i.e., solving the gasdynamics and then the chemistry through independent integration procedures), the decoupling of the convective waves does not lead to conservative fluxes. This is primarily due to the fact that the system does not take into account the effect of changing species densities on the velocity u when gasdynamics and chemistry are solved independently.

The method introduced here can be computationally intensive. Calculating $X_{j+\frac{1}{2}}\Phi_{j+\frac{1}{2}}$ at each midpoint is expensive, particularly if the number of species is large. For realistic gases with 11 species, $X_{j+\frac{1}{2}}$ and $X^{-1}_{j+\frac{1}{2}}$ are 13×13 matrices in one dimension and are involved in matrix multiplications. If the matrix algebra is not done efficiently, the number of operations grows as the cube of the matrix size. A method proposed in the following section reduces the computational requirement significantly and grows only linearly with the number of species.

Modified Dissipation Operator

A modified form of Eq. (19) is used to reduce the computation requirements when additional species are added. A new numerical dissipation is added that retains all of the conservation properties and is fully coupled. Yet, the method resembles that for a decoupled system. Equation (19) is rewritten

$$\tilde{F}_{j+\frac{1}{2}}=\tfrac{1}{2}\left[F_j+F_{j+1}+\left(\mathscr{L}_{j+\frac{1}{2}}\tilde{X}_{j+\frac{1}{2}}\tilde{\Phi}_{j+\frac{1}{2}}+\Sigma\right)\right] \tag{26}$$

where the new numerical dissipation is defined by $\mathscr{L}_{j+\frac{1}{2}}\tilde{X}_{j+\frac{1}{2}}\tilde{\Phi}_{j+\frac{1}{2}}+\Sigma$. The matrices $\tilde{X}_{j+\frac{1}{2}}$ and $\tilde{\Phi}_{j+\frac{1}{2}}$ correspond to the dissipation operator for only the gasdynamics equations, including conservation of the mixture-mass. The corresponding eigenvalues and eigenvectors for the gasdynamics equations alone are

$$\Lambda=\text{Diag}\left[u,\ u+\sqrt{P_\rho+P_E(H-u^2)},\ u-\sqrt{P_\rho+P_E(H-u^2)}\right] \tag{27}$$

$$\tilde{X}=\begin{bmatrix} 1 & 1 & 1 \\ u & u+a & u-a \\ H-\frac{a^2}{P_E} & H+ua & H-ua \end{bmatrix} \tag{28}$$

$$\tilde{X}^{-1}=\begin{bmatrix} 1-\frac{P_\rho}{a^2} & u\frac{P_E}{a^2} & -\frac{P_E}{a^2} \\ \frac{1}{2a^2}(P_\rho-ua) & \frac{1}{2a^2}(a-uP_E) & \frac{1}{2a^2}P_E \\ \frac{1}{2a^2}(P_\rho+ua) & -\frac{1}{2a^2}(a+uP_E) & \frac{1}{2a^2}P_E \end{bmatrix} \tag{29}$$

The conservative variables for the gasdynamics equations alone are $q=[\rho, m, E]'$ and $\tilde{\Phi}$ is defined by Eq. (23). With this new dissipation model, the momentum and energy equations receive the same amount of numerical damping, but the species equations must use the damping from the mixture-mass equation. The operator $\mathscr{L}_{j+\frac{1}{2}}$ distributes this dissipation depending on the mass fraction. $\mathscr{L}_{j+\frac{1}{2}}$ is defined by

$$\mathscr{L}=\begin{bmatrix} c_1 & 0 & 0 \\ c_2 & 0 & 0 \\ c_3 & 0 & 0 \\ 0 & 1 & 0 \\ 0 & 0 & 1 \end{bmatrix} \tag{30}$$

This part of the dissipation operator assures that the mixture-mass equation is conserved and effectively upwinded. On the other hand, the species equations are not receiving the proper amount of dissipation. A correction term Σ is added for the species equations.

If the equations had been solved decoupled (i.e., as sets of gasdynamics and of species conservation equations), the species equations would take on the following form:

$$\frac{\partial \rho_i}{\partial t}+u\frac{\partial \rho_i}{\partial x}=w_i \tag{31}$$

If the TVD dissipation operator were used on the uncoupled equations, then

$$X_{j+\frac{1}{2}}\Phi_{j+\frac{1}{2}}=u_{j+\frac{1}{2}}(\rho_{i,j+1}-\rho_{i,j}) \tag{32}$$

This simple expression, as mentioned previously, will not result with mixture mass conservation. It is, however, convenient to use as a correction factor. First, define

$$\omega=u_{j+\frac{1}{2}}\sum_{i=0}^{ns}(q_{i,j+1}-q_{i,j}) \tag{33}$$

and then

$$\Sigma=\begin{bmatrix} c_1\omega-u_{j+\frac{1}{2}}(\rho_{1,j+1}-\rho_{1,j}) \\ c_2\omega-u_{j+\frac{1}{2}}(\rho_{2,j+1}-\rho_{2,j}) \\ c_3\omega-u_{j+\frac{1}{2}}(\rho_{3,j+1}-\rho_{3,j}) \\ 0 \\ 0 \end{bmatrix} \tag{34}$$

With this correction, all of the coupling and conservation properties are accounted for. The terms in Σ all sum to zero, therefore preserving the conservation of the mixture mass; yet, each species has its own, correct dissipation. The computation of the dissipation operator is now linear with the number of species and involves only the 3×3 matrices of the gasdynamics equations. This procedure has been used successfully and is shown in the results.

Finite-Rate Chemistry

The source terms in Eq. (1) are a result of such chemical reactions as dissociation and recombination. The model reactions that will be presented here use a simple rate equation for dissociation/recombination similar to that found in Vincenti and Kruger.[9] For simplicity, only two species will be allowed to interact, with all others being inert.

The model dissociation reaction is described by

$$A_2+B\xrightarrow{k_f}2A+B-h^0_{A-A_2} \tag{35}$$

where an A_2 molecule dissociates as a result of a collision with molecule B and $h^0_{A-A_2}$ is the heat absorbed by the reaction. Species B can be either a molecule of A_2, A, or a third species. The equation for the forward reaction, to produce species A, is written

$$\left(\frac{dc_A}{dt}\right)_f=\sum_{i=0}^{ns}k_{f_i}c_{A_2}c_i \tag{36}$$

where k_{f_i} are the forward reaction rate constants and are defined by

$$k_{f_i}=C_{f_i}T^{\eta_{f_i}}e^{-\Theta_{d_i}/T} \tag{37}$$

For this study, the constants of Eq. (37), C_{f_i}, η_{f_i}, and Θ_{di}, are selected to define example chemical relaxation times and new equilibrium states. There is a set of constants for each type of collision, since it is assumed that collisions with any type of molecule, whether A_2, A, or B, produce a reaction.

Not all of the reactions produce molecule A. The reverse reaction, which produces A_2 from A, proceeds at such a rate that an equilibrium state is ultimately reached. The reverse, or backward reaction, has a rate defined by

$$\left(\frac{dc_{A_2}}{dt}\right)_b=\sum_{i=0}^{ns}k_{b_i}c_A^2c_i \tag{38}$$

where c_A is raised to the second power because two atoms of A must collide to form a molecule of A_2. The rate constants, k_{b_i}, are defined by

$$k_{b_i}=C_{b_i}T^{\eta b_i} \tag{39}$$

where, again, C_{b_i} and η_{b_i} are selected for a model gas.

The source terms for the dissociating, three-species model gas, where one gas is inert, is finally described by

$$W=\begin{bmatrix} -\rho\left(k_{f_{A_2}}c_{A_2}^2+k_{f_A}c_{A_c}c_A+k_{f_B}c_{A_2}-k_{b_{A_2}}c_A^2c_{A_2}-k_{b_A}c_A^3-k_{b_B}c_A^2c_B\right) \\ \rho\left(k_{f_{A_2}}c_{A_2}^2+k_{f_A}c_{A_2}c_A+k_{f_B}c_{A_2}c_B-k_{b_{A_2}}c_A^2c_{A_2}-k_{b_A}c_A^3-k_{b_B}c_A^2c_B\right) \\ 0 \\ 0 \\ 0 \end{bmatrix} \tag{40}$$

The results shown in this paper use a fourth-order Runge-Kutta procedure for integrating the source terms. A simple explicit Euler differencing has also proved to be adequate for the problems presented here. In general, however, explicit handling of the source terms runs into stability problems when approaching equilibrium conditions across a shock wave. This study does not encounter these problems because the reaction times across the shock are of the same order as the fluid flow times and, thus, do not dictate stability. Realistic problems, however, have chemical scales that differ by orders of magnitude and, therefore, implicit, exponential, or asymptotic handling of source terms is required. It is not the purpose of this paper to study numerical methods for stiff source terms.

Source Term Discontinuities

Numerical handling of the source terms is extremely difficult and warrants more research. One difficulty arises when the source terms jump at discontinuities. Evaluating W before a one-dimensional shock at equilibrium gives $W = 0$. Through the shock itself there is a large temperature rise, resulting in a flow out of chemical equilibrium. For realistic, hypervelocity flows the source term W will jump to values that can be orders of magnitude larger than the flux terms. The source term will decay after a certain distance, depending on the Damköhler number (the ratio of the chemical reaction rate to the flow rate) to zero at equilibrium. If the reaction rate is slow, the flow can remain frozen and the source term will decay very slowly. If the reaction rate is fast, compared to the characteristic speed of the flow, the species concentrations will relax to equilibrium quickly. It should be noted, however, that for real gases the reaction rate model presented earlier does not, in general, give equilibrium flow as a limiting case. This is a weakness of the reaction rate models.

The differencing at the discontinuity is critical. If central differencing is used for the flux terms, then the fluxes computed on the downstream side would be from flow that may be in strong nonequilibrium. This state would then propagate the influence upstream. However, with purely upwind differencing at the discontinuity the downstream reactions cannot affect the solution upstream. This differencing is one advantage of TVD operators, which limit the fluxes to upwind differencing at discontinuities. It was observed, through numerical experimentation, that any downstream influence just before the shock would quickly become noticeable throughout the flow.

Initial Conditions and Boundary Conditions

The computations are performed on a one-dimensional flow. The solution is initiated by providing an ideal-gas at the 25% point of the grid. The grid uses 75 equally spaced points and no effort is made in grid refinement. An initial discontinuity must be specified; otherwise, there would be no mechanism for a shock wave to form.

The upstream boundary uses Dirichlet data since all information is inflowing and all of the data must be specified. All of the results shown in this paper use an upstream Mach number of 30. The equations are normalized by freestream values so that upstream conditions are simple. The downstream data, on the other hand, are much more difficult. Dirichlet numbers for all downstream data are inappropriate, since all of the eigenvalues, except $u - a$, suggest the use of outflow conditions. Therefore, data are extrapolated from the interior of the grid. The negative eigenvalue, $u < a$ so $u - a < 0$, is the characteristic that lets the information propagate upstream and form a shock wave. Thus, at least one piece of information must be specified downstream to maintain the shock. In this study, the speed of sound is selected. Other variables such as pressure can be used, but the speed of sound requires less accuracy and, therefore, is favored.

The one-dimensional nature of the problem results in an physically sensitive shock. If the jump conditions are incorrect for a given Mach number and selected gas properties, then the shock wave must move to compensate. There is no way to stop the shock from moving except to correct the downstream boundary condition. Therefore, with inaccurate boundary conditions, the shock wave will eventually propagate out of the computational domain. The results obtained below use boundary conditions that are determined by varying the downstream speed of sound until the shock velocity approaches zero.

The difficulty of stabilizing the shock location can be avoided by computing a one-dimensional nozzle. The shock will stabilize by moving to a location where the jump conditions are correct. This approach has problems of its own, however. To investigate a Mach 30 shock wave, a nozzle requires an area expansion ratio of greater than 500 : 1. Including such expansions in a computational scheme represents an entirely different area of research.

Results

Results have been obtained for two model chemically reacting gases. The first gas simulates a pure dissociating gas with the concentration of A_2 initially 100%. The second gas roughly simulates air with 75.6% of molecule B, 24.4% of molecule A_2, and 0.0% of molecule A. These mass fractions represent those of N_2, O_2, and O in a standard atmosphere. In the second gas, molecule B is inert.

The reaction rates for the modeled gases have been selected so that A_2 dissociates 100% to A through a Mach 30 shock. Table 1 lists the constants used in this study. These rates are not necessarily the correct physical rates for dissociating O_2, but have been selected to illustrate the algorithm. They have been normalized with respect to freestream conditions, which accounts for the different exponents than one usually encounters. The species properties are found from simple gas models. The specific heat at constant pressure, C_p (normalized with respect to R, the gas constant), are $C_{p_B} = C_{p_{A_2}} = (2 + 5)/2$ and $C_{p_A} = (2 + 3)/2$. This simple model assumes there are five degrees of freedom for the diatonic molecule and three for the atom. The molecular masses have been normalized with respect to freestream continuous and have been selected to reflect the massive ratios of N_2, O_2, and O.

Figure 2 demonstrates the solution using different characteristic temperatures Θ_d in Eq. (37). Three examples, showing the effect of different Θ_d, are computed using the first model gas. The computation with $\Theta_d = 1500$ shows a solution that approaches equilibrium quickly. The chemical relaxation occurs over roughly four grid points which, for finite-difference procedures, can be considered to be close to the shock thickness. This relaxation rate represents the limit for a stable solution based on a CFL number $(u + a)(\Delta t/\Delta x)$ of 0.4, which was used for all calculations presented here. This rate demonstrates that the stiffness of the species production terms is no worse a factor than the flux terms for nearly

Table 1 Gas properties

Species	c_i,%	$\frac{M_i nfty}{M_i}$	$\frac{c_{p_i}}{R/M_i}$	C_f	η_f	C_b	η_b	θ_d	h_i^0
			a) gas 1, 100% A_2						
A_2	100	1.0	3.5	2×10^6	−1.5	10	−1	(a)	—
A	0	2.0	2.5	2×10^7	−2.0	10	−1.5	(a)	(b)
			b) gas 2, air model						
A_2	22.4	0.9055	3.5	2×10^6	−1.5	10	−1	535	—
A	0	1.8110	2.5	2×10^7	−2.0	10	−1.5	535	100
B	75.6	1.0349	3.5	2×10^5	−1.5	100	−1	535	—

[a] $\theta_d = 1500, 535, 225$. [b] $h^0 = 0, 100, 200$.

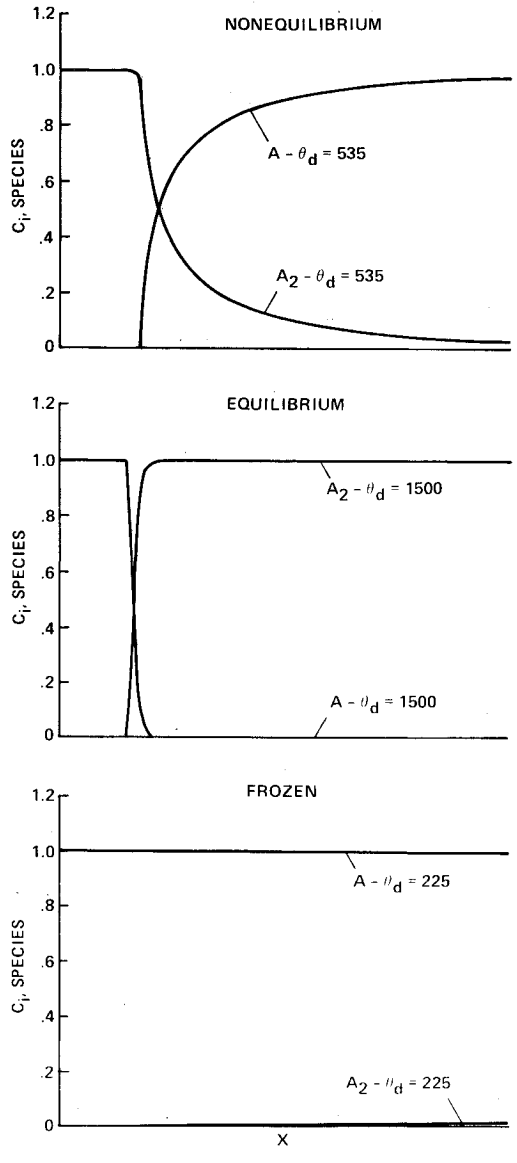

Fig. 2 Two-species gas dissociating through a one-dimensional, Mach 30 shock wave.

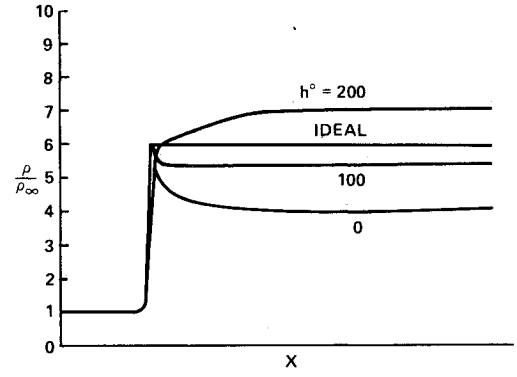

Fig. 3 Effect of heat of formation on density.

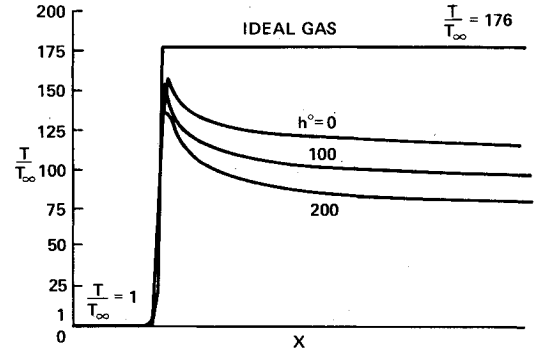

Fig. 4 Effect of heat of formation on temperature.

the computation. The final reaction rate, $\Theta_d = 225$, approaches the limit of frozen flow where the reaction time is long compared to the characteristic time of the flow. For the model gas with dissociation, the method presented in this paper appears capable of handling reaction rates that range from frozen flow to near equilibrium flow.

equilibrium flows. The second reaction rate uses $\Theta_d = 535$ and gives full dissociation in the characteristic length chosen for

Figures 3 and 4 demonstrate the effects of changes in heat of formation. Figure 3 shows the density and Fig. 4 the temperature. The density jumps to almost 6.0, the hypersonic limit, for an ideal-gas calculation with γ equaling the ratio of specific heats, which is 1.4. When the real gas is computed with no heat of formation, the density relaxes after the shock to a lower value. This lowering of the density is a result of the change from the diatomic gas to the dissociated gas, which has half the mass. There is also a lowering of the temperature due to dissociation. Pressure, however, is not affected by the dissociation, since the lowering of ρ and T in Eq. (3) is balanced by an increase in the mixture gas constant, $\sum_{i=1}^{ns} c_i(R/M_i)$. When the heat of formation is included in the definition of energy [Eq. (4)], the temperature continues to drop since energy is being removed from internal energy and transferred to chemical energy. However, the density increases. These trends continue as the heat of formation increases and eventually result in a density jump greater than expected for an ideal gas. Since pressure is not affected by the reaction, the decrease in temperature must be balanced by an increase in density.

Hypersonic approximations to the Rankine-Hugoniot jump conditions quickly give an indication of the accuracy of the method. If 100% dissociation is assumed, then the jump conditions are approximately

$$(c_pT)_2 \approx \tfrac{1}{2}u_1^2 - h_2^0 \tag{41}$$

where subscript 1 stands for the upstream conditions and subscript 2 for the downstream condition. The term h^0 is the total energy absorbed through the heat of formation for completely dissociated A_2. Using the approximation of Eq. (41), the ideal gas jump T_2/T_1 is 180, which is close to the value computed (the exact value is 176). The approximate equilibrium jump conditions are 126, 102, and 78 for h^0 equals 0, 100, and 200, respectively. These aproximate values compare favorably with the asymptotic values of Fig. 4.

The second model gas was computed using both the fully coupled method and the modified method. The conditions for this gas are shown in Table 1b, and the resulting species distributions are shown in Fig. 5. Both procedures successfully capture the shock and are virtually identical. There is a slight difference in the crispness at the shock point, however. This slight difference is negligible and appears not to affect other areas of the flow. A 60% reduction of computer time was found in computing the numerical dissipation terms with the modified method. For the model gases studied here and the fourth-order Runge-Kutta procedure for the source terms, the computation time is dominated by the source terms, thus,

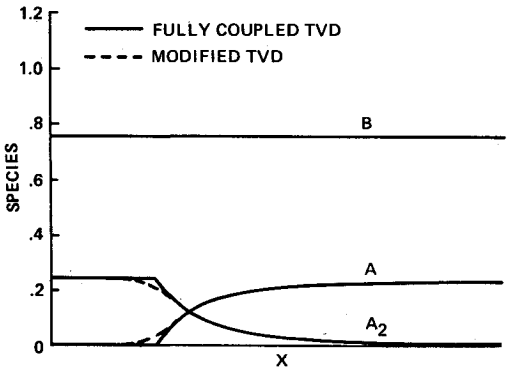

Fig. 5 Three-species gas through a one-dimensional shock wave.

the improvement in overall computer times is not large. It should be noted that the overall computation time for 1000 iterations and 75 grid points is under 20 s on the Cray X-MP for either method.

The two test cases studied show the expected results from these simple examples. The authors believe that the method presented can be used to reliably predict the physics of chemically reacting flows. A future step will be to validate the algorithm, using physical gas constants, with real shock-tube data.

Conclusions

A method for solving chemically reacting flows at high Mach numbers has been presented. The method successfully captures strong, crisp shocks and includes the solution of individual species concentrations. The method is independent of the number of species and can allow one or more of the species to vanish without introducing new errors or singularities. Generalized, reacting gas characteristics have been evaluated for the complete coupled system. The hyperbolic nature of the time-dependent Euler equations allows these characteristics variables to be used to determine the wave propagation properties and is the motivation for using the TVD numerical dissipation.

Although coupled and therefore fundamentally correct, the method may become too expensive to compute for systems with a large number of species. The modified method presented in this paer overcomes this problem, since the computation of the TVD dissipation terms grow only linearly with the number of species. However, the computational requirements of the source terms also represent a dominant factor in determining the computer time and must be considered to achieve large savings. When using explicit Euler for source term integration, the CPU time savings of the modified method for three species was 60%. The fourth-order Runge-Kutta, on the other hand, saved only on the order of 10%. The modified method obtains identical results, except for crispness at the shock point, and is a less costly alternative to computing the fully coupled system.

References

[1]Menees, G.P., "Thermal Protection Requirements for Near-Earth Aeroassisted Orbital Transfer Vehicle Missions," *AIAA Progress in Astronautics and Aeronautics: Thermal Design of Aeroassisted Orbital Transfer Vehicles*, Vol. 96, edited by H.F. Nelson, 1985, pp. 257–285.

[2]Howe, J.T., "Introductory Aerothermodynamics of Advanced Space Transportation Systems," *Journal of Spacecraft and Rockets*, Vol. 22, Jan.–Feb. 1985, pp. 19–26.

[3]Harten, A. "A High Resolution Scheme for the Computation of Weak Solutions of Hyperbolic Conservation Laws," *Journal of Computational Physics*, Vol. 49, 1983, pp. 357–383.

[4]Yee, H.C., "Linearized Form of Implicit TVD Schemes for the Multidimensional Euler and Navier-Stokes Equations," *Advances in Hyperbolic Partial Differential Equations*, a special issue of *International Journal of Computer Mathematics with Applications*, Vol. 12A, No. 4/5, April/May, 1986, pp. 413–432.

[5]Park, C., "On Convergence of Computation of Chemically Reacting Flows," AIAA Paper 85-0247, Jan. 1985.

[6]Carofano, G.C., "Blast Computation Using Harten's Total Variation Diminishing Scheme," U.S. Army Research and Development Command, Tech. Rept. ARLCB-TR-84029, Oct. 1984.

[7]Bussing, T. R. A. and Murman, E. M., "A Finite Volume Method for the Calculation of Compressible Chemically Reacting Flows," AIAA Paper 85-0331, Jan. 1985.

[8]Yee, H.C., Warming, R. F., and Harten, A., "On a Class of TVD Schemes for Gas Dynamic Calculations," *Proceedings of INRIA Workshop on Numerical Methods for the Euler Equations of Fluid Dynamics*, edited by F. Angrand et al., SIAM, 1985, pp. 84–107.

[9]Vincenti, W. G. and Kruger, C. H., *Introduction to Physical Gas Dynamics*, Robert E. Krieger Publishing Comp., Malabar, FL, 1965 pp. 222–232.